

Auto-Prompting SAM for Mobile Friendly 3D Medical Image Segmentation

Chengyin Li¹, Prashant Khanduri¹, Yao Qiang¹, Rafi Ibn Sultan¹, Indrin Chetty², Dongxiao Zhu¹

¹Department of Computer Science, Wayne State University, dzhu@wayne.edu

²Henry Ford Health System

Abstract

*Segment Anything Model (SAM) has rapidly been adopted for segmenting a wide range of natural images. However, recent studies have indicated that SAM exhibits subpar performance on 3D medical image segmentation tasks. In addition to the domain gaps between natural and medical images, disparities in the spatial arrangement between 2D and 3D images, the substantial computational burden imposed by powerful GPU servers, and the time-consuming manual prompt generation impede the extension of SAM to a broader spectrum of medical image segmentation applications. To mitigate these challenges, we introduce a novel method, **AutoSAM Adapter**, designed specifically for 3D multi-organ CT-based segmentation. This approach utilizes parameter-efficient adaptation techniques and an automatic prompt learning paradigm, transforming SAM’s capabilities for 3D medical image segmentation. It eliminates the need for manual prompts and achieves SOTA performance in CT-based multi-organ segmentation tasks. Furthermore, we successfully transfer the acquired knowledge of the AutoSAM Adapter to other lightweight models tailored for 3D medical image analysis with enhanced performance. Through extensive experiments, the AutoSAM Adapter has been demonstrated as an effective method to adapt the foundational SAM-based 2D natural image segmentation model for 3D medical image segmentation tasks.*

1. Introduction

Recently, foundational models in computer vision, such as the Segment Anything Model (SAM), have significantly advanced the field of image segmentation [18]. SAM, in particular, has shown impressive performance and versatility across various semantic segmentation tasks [44], offering new potential for medical image segmentation, an area often limited by the availability and quality of segmentation masks. Unlike custom-designed transformer models like UNETR [9], SwinUNETR [38], and FocalUNETR [20], which are typically trained on limited patient samples and masks, foundational models including SAM benefit from

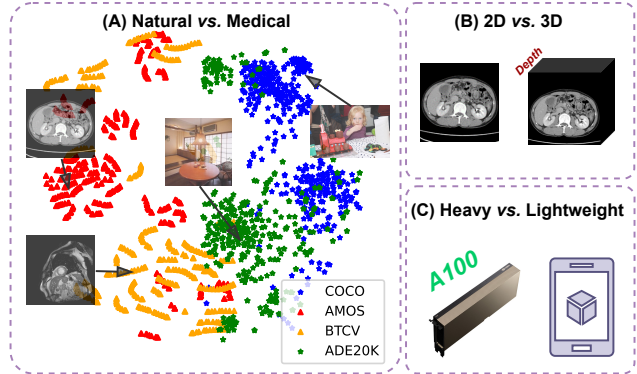


Figure 1. Challenges associated with using SAM for medical image segmentation include: (A) a T-SNE plot of embeddings encoded by SAM’s image encoder, showcasing differences between medical image datasets such as AMOS [15] and BTCV [19], and natural image datasets like ADE20K [48] and COCO [22]; (B) 2D vs 3D input; and (C) heavy vs lightweight computing requirements.

training on millions of images and billions of masks. However, despite their extensive training, these large-sized foundational models have been shown to underperform in medical image segmentation tasks when compared to SOTA models in this specific domain [6].

Recent efforts have attempted to extend the success of SAM to medical image segmentation tasks including [6, 24, 36, 41, 46]. However, the demonstrated performance has exhibited reduced precision and stability, particularly in more intricate segmentation tasks characterized by smaller sizes, irregular shapes, and lower contrast properties of medical images in comparison to natural images [6]. Adapting the original SAM architecture, which is rooted in 2D natural images, to effectively harness the 3D spatial information inherent in volumetric medical data poses a significant challenge. Novel approaches must be devised to bridge the gap between natural and medical image segmentation tasks, opening doors for the development of cutting-edge segmentation techniques. A few substantial issues (Fig. 1) that need to be addressed in developing a SAM-based med-

ical image segmentation framework are (A) encompassing the oversight of substantial domain disparities between natural and medical images (Fig. 1A), (B) extracting 3D spatial information from volumetric medical images effectively (Fig. 1B), and (C) the high computational demands even during inference (Fig. 1C). Furthermore, SAM’s reliance on labor-intensive manually generated prompts [4, 36] hampers its successful application, particularly in multi-organ medical image segmentation tasks.

As healthcare becomes increasingly patient-centered and portable imaging devices like Computed Tomography (CT) and Magnetic Resonance Imaging (MRI) become more accessible, point-of-care tests (POCT) hold significant potential to enhance treatment effectiveness and efficiency by providing diagnoses at the patient’s location. Especially in time-sensitive scenarios, POCT can substantially improve diagnosis and treatment processes, resulting in smoother and more efficient experiences for both patients and caregivers. Notably, portable 3D medical image segmentation techniques drive the functionality of POCTs, demanding the development of highly compressed models without compromising the segmentation performance.

To address the above issues, we introduce a novel **AutoSAM Adapter** method for a transition of SAM from 2D natural image to 3D for medical image segmentation. Initially, we design intricate modifications for the image encoder at the input level, enabling the original 2D transformer to adeptly accommodate volumetric inputs while optimizing the reusability of pre-trained weights with a parameter-efficient fine-tuning method. Subsequently, at the prompt encoder level, we design an Auto Prompt Generator (APG) module that takes the extracted feature maps from the previous image encoder as input and automatically learns the required prompts for the following mask encoder. This design effectively removes the time-consuming manual prompt generation process, especially, for multi-organ medical image segmentation tasks. Additionally, we prioritize a lightweight design for the mask decoder at the output level, emphasizing multi-layer aggregation. Through extensive experimentation on CT-based multi-organ segmentation datasets, inclusive of comprehensive comparisons with state-of-the-art approaches including nnUNet [14], as well as recent adapters in the field, our results exhibit a significant performance improvement over existing techniques. Finally, we utilize knowledge distillation (KD) [10] to transfer the learned knowledge from the AutoSAM Adapter to other lightweight segmentation models like SwinUNETR [38] (e.g., small and tiny version) for the resource-aware POCT use scenario. The main contributions of this work are summarized below.

- We adapt the 2D SAM model for 3D medical image segmentation with parameter-efficient fine-tuning, mitigating the gaps from 2D natural images to 3D medical images.

- We introduce an automated system (APG) to eliminate the laborious manual prompting process, simplifying the multi-organ medical image segmentation tasks.
- We conduct extensive experiments and analysis on three public and one private multi-organ segmentation datasets, demonstrating that the proposed **AutoSAM Adapter** achieves superior performance in medical image segmentation tasks compared to the SOTAs.
- We employ knowledge distillation to facilitate the transfer of learning from our AutoSAM Adapter to smaller, resource-efficient models, bridging the gap between complex models and practical medical imaging needs.

2. Related Work

Foundation computer vision models. The recent past has seen the emergence of numerous computer vision backbones pre-trained using various algorithms and datasets [5]. With advancements in these deep learning models, most contemporary vision frameworks adhere to the pre-training and fine-tuning paradigm [27]. Very recently, computer vision researchers have shown substantial interest in large and adaptable foundational models, capitalizing on pre-training techniques such as self-supervised learning [17], contrastive learning [40], and language-vision pre-training [33], among others. Notably, the SAM model [18], recently pre-trained on a dataset of over 11 million images, has emerged as a versatile foundational model for natural image segmentation. SAM demonstrates impressive zero-shot capabilities in segmenting diverse subjects in real-world environments, using an interactive and prompt-driven approach. Additionally, SEEM [50], another contemporaneous effort to SAM, introduces a more comprehensive prompting scheme to facilitate semantic-aware open-set segmentation. Furthermore, DINOv2 [29] focuses on scaling up the pre-training of a ViT model in terms of data and model size. This approach aims to generate versatile visual features that simplify the fine-tuning of the downstream tasks.

Parameter-efficient model fine-tuning. Given the extensive utilization of foundational models, the concept of parameter-efficient fine-tuning has garnered significant attention. Existing methods for efficient fine-tuning can be categorized into three groups [2]. Addition-based methods that involve incorporating lightweight adapters [30, 39] or prompts [16, 23] into the original model, with the sole focus on adjusting these parameters; Specification-based methods [7, 42] that concentrate on selecting a small subset of the original parameters for tuning; and reparameterization-based methods [12] that leverage low-rank matrices to approximate parameter updates. In recent times, a few researchers have extended pre-trained image models to encompass video comprehension [30] or volumetric segmentation [39]. Nevertheless, these methods treat the additional dimension as a “word group” and employ specialized mod-

ules to aggregate information along the word dimension. In contrast, in our work, we consider all three dimensions as isotropic and directly adapt the trained transformer block to capture 3D patterns.

SAM-based medical image segmentation. This line of work primarily focuses on enhancing SAM through fine-tuning for specific segmentation datasets, aiming to mitigate the noticeable performance drop of SAM on medical images [13]. MedSAM [24] specifically concentrated on refining the SAM decoder by employing prompts generated from label masks across more than 30 medical image datasets. The outcome demonstrated improved performance compared to zero-shot predictions using prompts. Zhang et al. [45] optimized for a low-rank fine-tuning approach, focusing on the SAM encoder. By combining this strategy with SAM decoder training, they tailored SAM for abdominal segmentation tasks. Tal et al. [36], redesigned the SAM’s prompt encoder by taking the original 2D medical image as input. SAM-Med2D [1] attempted to fine-tune SAM with a large collection of 2D medical image datasets. The work reported in Wu et al. [41] takes a different approach, starting with pre-training the entire encoder through self-supervised learning on collected datasets for downstream medical image segmentation tasks. Despite some progress, existing methods tend to overlook the 3D pattern of medical images, rely on extensive pre-training, and/or involve laborious manual prompting processes. These limitations hinder the realization of the full potential of SAM in CT-based 3D multi-organ segmentation tasks. The closest work to ours is the 3DSAM-Adapter [6], in which only the tumor segmentation task is performed on each type of tumor individually with a time- and labor-consuming prompting requirement. As such, their approach has not been evaluated on the more challenging multi-organ segmentation task with minimal human intervention.

Lightweight models for POCT. Applying the SAM model for medical segmentation in Point-of-Care Testing (POCT) scenarios is challenging due to limited computational resources. To address this, several efficient learning approaches have been proposed. Initial strategies involved pruning the network to retain only crucial connections and quantizing weights for weight sharing [8]. Subsequent efforts focused on creating custom neural network architectures like Mobile ViT [26], MobileNet [11], and EfficientNet [37], designed for on-device training and inference, prioritizing reduced model size over performance. An emerging strategy involves compressing large models into lightweight ones during training, a process that does not significantly compromise performance. Knowledge distillation (KD) [10] exemplifies this approach. Here, a comprehensive teacher model is first trained on powerful hardware, and then a student model is trained on a mobile device, acquiring ‘knowledge’ from the teacher via soft la-

bels. The student model not only learns to replicate the teacher model’s outputs but also minimizes the loss between true labels and predictive probabilities. This KD method produces compact student models with impressive performance in various real-world applications, such as COVID-MobileXpert [21] and on-device text classification [31]. Recently, this technique has been adapted to develop mobile versions of SAM [43].

3. Method

In this section, we explain how to modify the original SAM architecture, initially developed for 2D natural images, to work with 3D volumetric medical images for segmentation tasks. We begin by offering a brief overview of the SAM framework (as depicted in Fig. 2), followed by a detailed explanation of the adjustments made to the image encoder, prompt encoder, and mask decoder.

3.1. The SAM Architecture

SAM [18] is a prompt-driven image segmentation framework, renowned for its exceptional performance in segmenting natural images. The architecture of SAM comprises three key components: an image encoder, a prompt encoder, and a mask decoder. The image encoder utilizes the Vision Transformer (ViT) [3, 32] to transform original images into one-time image embeddings. The prompt encoder skillfully converts various types of prompts – including foreground/background points, rough boxes or masks, clicks, text, or any information indicating the target of segmentation – into compact embeddings. These embeddings from both the image and prompt encoders are then seamlessly integrated by the mask decoder to produce accurate segmentation masks.

Although SAM has been successful in 2D natural image segmentation, it faces significant challenges when applied to 3D volumetric medical imagery. A key issue is the model’s reliance on slice-wise predictions, which fail to consider the inter-slice spatial context, thereby impacting its suitability for complex medical tasks. Additionally, the inherent domain disparities between medical and natural images contribute to its performance limitations in medical applications. To effectively address these challenges and optimize SAM for medical imaging tasks, tailored adaptation, and fine-tuning of the model become essential.

3.2. Handling 3D Medical Inputs

To enhance SAM’s capability in processing 3D medical images, we propose an adaptation strategy named **AutoSAM Adapter**, as illustrated in Fig. 2A. This strategy has two primary objectives: firstly, to enable the model to directly learn 3D spatial patterns, and secondly, to ensure continuity by inheriting most parameters from the pre-trained model

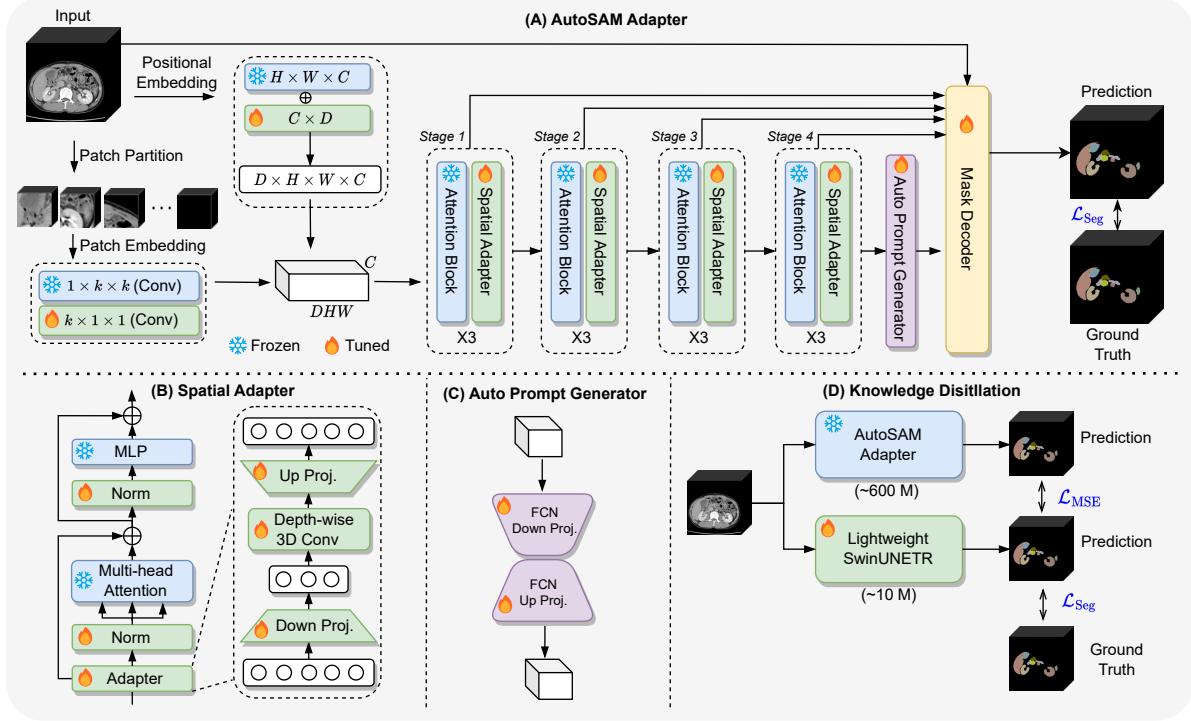


Figure 2. (A) The overall architecture of the **AutoSAM Adapter**, (B) the design of the **Spatial Adapter** module, which utilizes parameter-efficient model fine-tuning, (C) the architecture of the **Auto Prompt Generator**, featuring a U-Net-like encoder-decoder design, and (D) the pipeline for deriving a lightweight SwinUNETR from the fine-tuned AutoSAM Adapter, aided by the knowledge distillation process.

while introducing easily adjustable incremental parameters. The detailed design is elaborated as follows.

Positional encoding enhancement. In the pre-trained ViT model, there is a lookup table of size $C \times H \times W$ for positional encoding, where C represents the channel, H the height, and W the width. Additionally, we initialize a tunable lookup table of size $C \times D$ (with D representing the depth of a volume patch) with zeros. To obtain the positional encoding of a 3D point (d, h, w) , we add the embedding from the frozen lookup table with (h, w) to the embedding from the tunable lookup table with (d) .

Patch embedding adjustments. We utilize a combination of $1 \times k \times k$ and $k \times 1 \times 1$ 3D convolutions to approximate the effect of a $k \times k \times k$ convolution (e.g., kernel size $k = 14$). The $1 \times k \times k$ convolution is initialized with the weights from a pre-trained 2D convolution and remains unchanged during the fine-tuning phase. As for the newly introduced $k \times 1 \times 1$ 3D convolution, we apply depth-wise convolution to decrease the number of parameters that need adjustment. This approach helps in managing the complexity of the model.

Adapting attention block. The attention blocks can be directly adjusted to accommodate 3D features. In the case of 2D inputs, the size of the queries is $[B, HW, C]$, which can be effortlessly modified to $[B, DHW, C]$ for 3D in-

puts, while retaining all the pre-trained weights. We implement sliding-window mechanisms akin to those in the SwinUNETR [38] to mitigate the memory impact resulting from the increase in dimensions. This approach aids in optimizing the model’s performance while managing memory requirements.

Bottleneck modifications. Given that convolution layers are generally easier to optimize than transformers, we replace 2D convolutions in the bottleneck with 3D counterparts and train them from scratch to improve performance.

By making the above adjustments, we can smoothly transition the 2D ViT into a 3D ViT, reusing most parameters. However, fully fine-tuning the 3D ViT can be resource-intensive. To address this, we propose using a lightweight adapter approach for efficient fine-tuning. The adapter comprises a down-projection linear layer and an up-projection linear layer, represented as $\text{Adapter}(\mathbf{X}) = \mathbf{X} + \text{Act}(\mathbf{X}W_{\text{Down}})W_{\text{Up}}$. Here, $\mathbf{X} \in \mathbb{R}^{N \times C}$ is the original feature representation, $W_{\text{Down}} \in \mathbb{R}^{C \times N'}$ and $W_{\text{Up}} \in \mathbb{R}^{N' \times C}$ are down-projection and up-projection layers, and $\text{Act}(\cdot)$ is the activation function. To enhance 3D spatial awareness, we include a depth-wise 3D convolution after the down-projection layer, as shown in Fig. 2B. This enhancement improves the adapter’s utilization of 3D spatial cues.

Throughout the training phase, we exclusively adjust the

parameters of convolutions, spatial adapters, and normalization layers, while maintaining all other parameters in a frozen state. This frozen approach enhances memory efficiency during training. Fine-tuning the adapter and normalization layers aids in bridging the gap between natural images and medical images, enabling the model to adapt more effectively to the medical image domain.

3.3. Auto Prompt Generator

SAM initially applies positional embedding to both prompt (e.g., points or boxes) and image, ensuring that prompt and image embeddings at the same position share identical positional encoding. Subsequently, the prompt embedding engages in cross-attention with the image embedding, evolving from positional to semantic attributes. However, this cross-attention mechanism, while effective in 2D settings, can lead to over-smoothing issues when applied to 3D feature maps [6]. Adapting to 3D settings can significantly increase the number of tokens, potentially resulting in a uniform probability distribution.

Furthermore, prompt-based segmentation may not be well-suited for real-world applications due to two primary reasons. Firstly, it is time-consuming for multi-class scenarios, as seen in many medical image segmentation challenges requiring the segmentation of multiple classes simultaneously. This becomes particularly challenging for small or closely located organs. Secondly, segmentation quality heavily relies on the precision of the prompts, yet creating accurate prompts demands domain-specific expertise, often unavailable to non-expert users. These limitations diminish the practicality of prompt-based methods.

To overcome these limitations, we propose to use an Auto Prompt Generator (APG) instead of positional encoding to represent the prompt. The whole process is illustrated in Fig. 2C. Instead of using manually generated points or bounding boxes, we directly take the output feature map after the last block of attention and spatial adapter operation. This Auto Prompt Generator follows a fully convolutional neural (FCN) based encoder-decoder design that resembles 3D UNet [35]. This generator boasts a lightweight structure, leveraging 3D-based convolution operations, and can be effortlessly learned from scratch. This enables precise prompt generation tailored to different medical segmentation tasks. Notably, it eliminates the need for additional manually generated prompts, simplifying and expediting the multi-class medical image segmentation tasks.

3.4. Lightweight Mask Decoder

The mask decoder in SAM was originally designed to be lightweight, primarily using stacks of 2D convolution layers. In our updated version, we have replaced these 2D convolutions with 3D convolutions to enable direct 3D mask generation. The initial design of the decoder, which lacks

progressive upsampling and skip connections, is effective for natural images that typically feature large objects with distinct boundaries. However, in the context of volumetric medical image segmentation, it is well-recognized that U-shaped networks with skip connections at multiple levels are crucial for success [14, 38]. This is due to the smaller size of objects in medical images and their often indistinct boundaries, necessitating networks that can preserve higher-resolution details for better discrimination. Therefore, the use of U-shaped architectures with skip connections becomes imperative.

To address this need while keeping the design lightweight, we incorporate a multi-layer aggregation mechanism (MLAM) [6, 47] in our decoder. We utilize the intermediate feature maps from stages 1-4 (as depicted in Fig. 2A) of the image encoder, along with the prompt embedding from the auto prompt generator, to enrich the mask feature map without compromising efficiency. For improved resolution detail, we upsample the mask feature map to match the original resolution, then concatenate it with the original image. This concatenated map is fused using another 3D convolution to generate the final mask. This method effectively combines high-resolution details with the original image data in the mask generation process. We have streamlined the original SAM by focusing solely on a targeted downstream task and omitting features like multi-task generation and ambiguity awareness. The backbone of the mask decoder primarily comprises lightweight 3D convolutional layers, which are known for their ease of optimization. Consequently, we train all parameters of the decoder from scratch.

3.5. Knowledge Distillation

Despite our efforts to introduce modules that are significantly more lightweight than the original SAM, we still face challenges in reducing the weight complexity of SAM’s ViT encoder segment. This component of the encoder contains a substantial portion of the model’s parameters, which complicates the integration of the AutoSAM Adapter into POCT environments.

To overcome this, we leverage the effectiveness of Knowledge Distillation (KD) techniques (as shown in Fig. 2D) and the availability of medical segmentation-specific models. Our approach aims to transfer the accumulated knowledge (Equation 2) from the AutoSAM Adapter, which has approximately 600 million parameters, to a significantly smaller SwinUNETR model with around 10 million parameters. This strategy is designed to bridge the gap between complex, resource-intensive models and those that are more resource-aware, facilitating practical 3D medical image segmentation-based diagnosis directly at the patient’s location.

3.6. Loss Function

For training the AutoSAM Adapter (as shown in Fig. 2A), a combination of Dice loss and Cross-Entropy loss is used to assess the alignment between the predicted mask and the ground truth on a pixel-wise basis. The objective function for the segmentation head is defined as follows:

$$\mathcal{L}_{\text{Seg}} = \mathcal{L}_{\text{Dice}}(\hat{p}_i, g_i) + \mathcal{L}_{\text{CE}}(\hat{p}_i, g_i), \quad (1)$$

where \hat{p}_i represents the predicted voxel probabilities from the main task, and g_i represents the ground truth mask for an input volume i . The predicted probabilities, \hat{p}_i , result from applying the AutoSAM Adapter to the input 3D volume for the main task.

Regarding the KD process (as illustrated in Fig. 2D), we adopt the following total loss:

$$\mathcal{L}_{\text{tot}} = \lambda \mathcal{L}_{\text{Seg}} + (1 - \lambda) \mathcal{L}_{\text{MSE}}, \quad (2)$$

where \mathcal{L}_{MSE} is the mean square error between the predicted probabilities of the lightweight student model and AutoSAM Adapter teacher model, and λ serves as a hyperparameter regulating how much the lightweight SwinUNETR model should learn from both the prediction mask generated by the AutoSAM Adapter and the ground truth. This approach enables a transfer of knowledge from the AutoSAM Adapter to the SwinUNETR model while striking a balance between the two information sources.

4. Experiments

Datasets and evaluation. In our study, four CT datasets were utilized to evaluate 3D multi-organ segmentation models, comprising three public and one private institutional dataset. The **BTCV** [19] dataset includes 30 abdominal CT scans, annotating 13 organs across 24 training and 6 testing scans. The **AMOS** [15] dataset, with 300 multi-contrast abdominal CT scans, annotates 15 anatomies and is divided into 200 training and 100 testing scans. The **CT-ORG** [34] dataset consists of 100 CT scans, highlighting 5 organs, with a split of 81 for training and 19 for testing. Additionally, a private **Institutional Pelvic** dataset of 300 prostate cancer patients provides 3 manually annotated contours per case, distributed among 225 training, 30 validation, and 45 testing cases. This blend of datasets, including public and institutional sources, offers a comprehensive basis for assessing the performance of advanced segmentation models in varied medical scenarios. Dataset pre-processing is in the Appendix. Dice Similarity Coefficient (Dice) and Normalized Surface Distance (NSD) are evaluated for the multi-organ segmentation tasks.

Implementation details. The AutoSAM Adapter model is trained using the AdamW optimizer with a warm-up exponential decay scheduler of 200 epochs. The segmentation

experiments use a batch size of 1 per GPU with a patch size of $128 \times 128 \times 128$. Default initial learning rate of $5e^{-4}$, momentum of 0.9 and decay of $1e^{-5}$. The framework is implemented in MONAI 1.2¹ and PyTorch 2.0². Models are trained on a server with eight NVIDIA A100 cards. Foreground and background patches are randomly sampled at a 1 : 1 ratio. We select the best model with the highest Dice metric on the validation dataset or the final epoch’s model for a dataset without a predefined validation split, with empirical evidence of negligible gain via a 5-fold cross-validation strategy. Baseline models are trained from scratch following their default settings. For inference, an overlapping area ratio of 0.75 is applied via the sliding window strategy.

5. Results & Discussion

In this section, we would like to evaluate the performance of our proposed **AutoSAM Adapter** concerning both the task-specific SOTAs and the SAM-adopting-based methods. The effectiveness of different modules for our designs will be evaluated as well.

5.1. Comparison with SOTAs

We extensively compare our model with the SOTA 3D medical image segmentation approaches, including the most recent Transformer-based methods including UNETR [9], SwinUNETR [38], and nnFormer [49], as well as CNN-based methods such as nnUNet [14]. As indicated in Table 1, we observe that the proposed **AutoSAM Adapter** generally outperforms all other SOTA methods in both Dice and NSD metrics across all four datasets. Significant improvements are particularly noticeable in the BTCV dataset, with up to a 3% increase in the average Dice score and a 3% to 7% improvement in the average NSD metric. As the training sample size increases for the AMOS dataset compared to BTCV, the AutoSAM Adapter performs even better, achieving up to a 14% improvement in Dice and a 2% to 19% improvement in NSD. For the CT-ORG dataset, our model achieves the highest NSD and a competitive Dice score compared to other baselines. Notably, the AutoSAM Adapter consistently demonstrates a robust performance in real-world scenarios, as seen in its consistently superior performance on the private Institutional Pelvic dataset.

The superiority of our AutoSAM Adapter model is further highlighted by qualitative results. As depicted in Fig. 3, qualitative comparisons of the predicted masks from various segmentation models reveal that our AutoSAM Adapter yields visually superior mask predictions, particularly in terms of more accurate boundary delineation, when compared to its SOTA counterparts. In summary, while the

¹<https://monai.io/>

²<https://pytorch.org/>

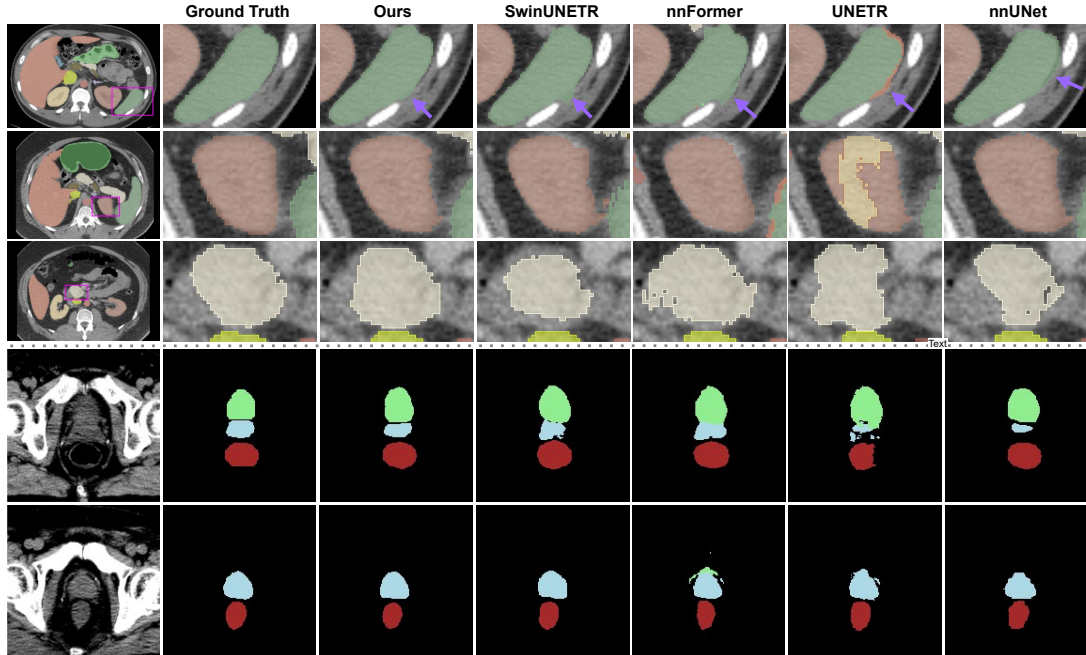


Figure 3. Qualitative visualizations compare our **AutoSAM Adapter** with baseline methods using three subjects from public datasets (Rows 1-3) and two subjects from the private Institutional Pelvic dataset (Rows 4-5). Enhanced areas in these visualizations illustrate improvements in segmenting the left kidney (light red) and pancreas (beige). Additionally, segmentation masks are shown for the prostate (blue), bladder (green), and rectum (red).

Model	Tuned Params. (M)	BTCV		AMOS		CT-ORG		Institutional Pelvic	
		mDice \uparrow	mNSD \uparrow	mDice \uparrow	mNSD \uparrow	mDice \uparrow	mNSD \uparrow	mDice \uparrow	mNSD \uparrow
nnUNet [14]	31.18	84.34	73.21	87.43	77.12	85.51	75.60	88.04	83.87
nnFormer [49]	150.14	83.51	71.65	84.52	70.06	82.75	70.31	87.60	82.13
UNETR [9]	93.02	85.47	74.35	77.24	60.58	83.13	71.56	86.68	81.54
SwinUNETR [38]	62.83	86.58	75.26	86.19	74.83	84.34	72.32	89.12	83.54
Ours	26.53	87.15	78.83*	88.65*	79.41*	85.12	76.37*	91.30*	84.35*

Table 1. Comparison of the overall performance between four STOs and our **AutoSAM Adapter** on four datasets. The best results are highlighted in bold font. (*: $p < 0.01$, with Wilcoxon signed-rank test to all SOTAs)

original SAM displayed relatively weaker performance in medical image segmentation tasks as compared to SOTA methods [25], our adapted design registers significant enhancements and generalization to 3D medical image segmentation.

5.2. Comparison with SAM-based Methods

We further compare our method with existing SAM-based methods for multi-class medical image segmentation, including the original SAM and MedSAM [24]. MedSAM can be implemented with either full fine-tuning or partial fine-tuning, where only the prompt encoder and mask decoder are updated using point prompts. Other adaptation methods were not considered, as they either require collecting a large number of medical images for fine-tuning (e.g., Medical-SAM-Adapter [41], SAM-Med2D [1]), or they do

Model	Tuning Option	BTCV		AMOS	
		mDice \uparrow	mNSD \uparrow	mDice \uparrow	mNSD \uparrow
SAM [18]	None	54.86	-	49.31	-
MedSAM [24]	P&M	80.65	66.82	70.28	59.61
MedSAM [24]	Full	84.57	73.76	83.10	70.26
Ours	P&M	87.15	78.83	88.65	79.41

Table 2. Comparison with SAM-based methods, where the best results are highlighted in bold. 'P&M' indicates only fine-tuning the prompt encoder and mask decoder, 'Full' denotes full fine-tuning, and 'None' represents no fine-tuning.

not specifically target multi-organ segmentation tasks (e.g., 3DSAM-Adapter [6]).

The outcomes are meticulously outlined in Table 2, underscoring how our adaptation strategy surpasses all existing methods. Notably, our approach outshines the

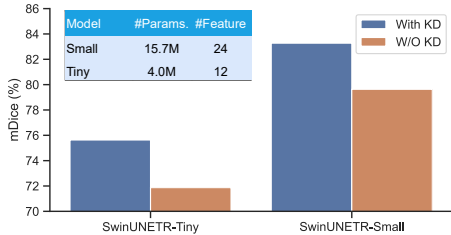


Figure 4. The comparison of the Dice metric on the BTCV dataset with/without using the KD for lightweight models.

second-best technique by a margin of 3% in terms of BTCV segmentation Dice, 5% for NSD, and 6% concerning AMOS segmentation Dice, accompanied by a substantial 9% for NSD. Impressively, it even outperforms the complete fine-tuning variant of MedSAM, even when considering parameter-efficient fine-tuning. These results effectively validate our hypothesis that parameters pre-trained on 2D images can be effectively harnessed to grasp 3D spatial features with only minor adjustments. Moreover, our approach of treating all dimensions equivalently emerges as a superior strategy compared to interpreting the depth dimension as a distinct group in the context of medical image segmentation.

5.3. Lightweight Models via Knowledge Distillation

To address the requirement for lightweight models in the context of POCT, we have taken a further step towards compressing the AutoSAM Adapter into lightweight SwinUNETRs (specifically, the tiny- or small-version) using a simple yet effective KD process, as illustrated in Fig. 2D. For the experiments, the tuning parameter λ has been set to 0.5 for the KD learning process. Other training strategies remain consistent with those employed in optimizing the AutoSAM Adapter. The outcomes of BTCV’s average Dice scores, both with and without the utilization of KD, are shown in Fig. 4. Compared to their KD-absent counterparts, models incorporating KD demonstrate a marked improvement in the average Dice scores. Specifically, SwinUNETR-Tiny (with a feature size of 12 and 4.0M parameters) displays an approximate 4% enhancement, while SwinUNETR-Small (with a feature size of 24 and 15.7M parameters) exhibits a comparable advancement.

5.4. Ablation Study

Effects of APG and MLAM. The Auto Prompt Generator (APG) in our AutoSAM Adapter refines the feature maps from the final stage of the attention block in the image encoder, paralleling the way the original SAM’s prompt encoder processes manual prompts. Without APG, these feature maps are directly fed into the mask decoder. Beyond APG, a Multi-Layer Aggregation Mechanism (MLAM) is

APG	MLAM	mDice \uparrow	mNSD \uparrow
✓	✓	87.15	78.83
✗	✓	85.23	74.12
✓	✗	84.37	73.54
✗	✗	81.14	70.33

Table 3. Ablation study evaluating the effectiveness of the Automated Prompt Generator (APG) and Multi-Level Attention Mechanism (MLAM) designs in our **AutoSAM Adapter**.

also applied for the integration of information from various stages of the encoder and APG to the final mask decoder. To evaluate the effectiveness of both APG and MLAM, we conducted a comparative analysis using the BTCV dataset by removing these components. The findings, presented in Table 3, reveal significant improvements in both Dice and NSD metrics when APG and MLAM are employed. These results highlight the substantial contribution of APG and MLAM to enhancing the efficacy of medical image segmentation.

Effects of λ for Knowledge Distillation. By adjusting the parameter λ in Equation 2, we can modify the weight given to learning from the ground truth or the AutoSAM Adapter teacher in the SwinUNETR-small model (BTCV dataset). As λ increases, we initially observe an increase in performance, which then decreases after λ reaches 0.5, as shown in Table 4.

λ	0	0.2	0.5	0.8	1.0
mDice \uparrow	78.54	82.45	83.27	81.14	79.63

Table 4. The impact of λ on the Knowledge Distillation (KD) process.

6. Conclusion

In this study, we introduce the AutoSAM Adapter for CT-based 3D multi-organ medical image segmentation, which adapts the 2D Segment Anything Model (SAM) to handle the complexities of 3D imaging. Our approach effectively mitigates challenges such as domain differences, spatial disparities, and computational demands through parameter-efficient adaptation and automated prompt generation. Additionally, the integration of knowledge distillation further enhances the performance of other lightweight 3D segmentation models. Comprehensive experiments have validated the effectiveness of the AutoSAM Adapter, marking it as a significant advancement in medical image segmentation.

Limitations. While our AutoSAM Adapter achieved superior performance in multi-organ segmentation tasks, certain limitations should also be noted. Our approach does not consider the pre-training of the image encoder via collecting a huge amount of medical images, nor does it focus on creating a universally adaptable model for multiple different datasets. Further related research would be worthwhile.

References

- [1] Junlong Cheng, Jin Ye, Zhongying Deng, Jianpin Chen, Tianbin Li, Haoyu Wang, Yanzhou Su, Ziyang Huang, Jilong Chen, Lei Jiang, et al. Sam-med2d. *arXiv preprint arXiv:2308.16184*, 2023. [3](#), [7](#)
- [2] Ning Ding, Yujia Qin, Guang Yang, Fuchao Wei, Zonghan Yang, Yusheng Su, Shengding Hu, Yulin Chen, Chi-Min Chan, Weize Chen, et al. Parameter-efficient fine-tuning of large-scale pre-trained language models. *Nature Machine Intelligence*, 5(3):220–235, 2023. [2](#)
- [3] Alexey Dosovitskiy, Lucas Beyer, Alexander Kolesnikov, Dirk Weissenborn, Xiaohua Zhai, Thomas Unterthiner, Mostafa Dehghani, Matthias Minderer, Georg Heigold, Sylvain Gelly, et al. An image is worth 16x16 words: Transformers for image recognition at scale. *arXiv preprint arXiv:2010.11929*, 2020. [3](#)
- [4] Yifan Gao, Wei Xia, Dingdu Hu, and Xin Gao. Desam: Decoupling segment anything model for generalizable medical image segmentation. *arXiv preprint arXiv:2306.00499*, 2023. [2](#)
- [5] Micah Goldblum, Hossein Souri, Renkun Ni, Manli Shu, Viraj Prabhu, Gowthami Somepalli, Prithvijit Chattopadhyay, Mark Ibrahim, Adrien Bardes, Judy Hoffman, et al. Battle of the backbones: A large-scale comparison of pre-trained models across computer vision tasks. *arXiv preprint arXiv:2310.19909*, 2023. [2](#)
- [6] Shizhan Gong, Yuan Zhong, Wenao Ma, Jinpeng Li, Zhao Wang, Jingyang Zhang, Pheng-Ann Heng, and Qi Dou. 3dsam-adapter: Holistic adaptation of sam from 2d to 3d for promptable medical image segmentation. *arXiv preprint arXiv:2306.13465*, 2023. [1](#), [3](#), [5](#), [7](#)
- [7] Demi Guo, Alexander M Rush, and Yoon Kim. Parameter-efficient transfer learning with diff pruning. *arXiv preprint arXiv:2012.07463*, 2020. [2](#)
- [8] Song Han, Huizi Mao, and William J Dally. Deep compression: Compressing deep neural networks with pruning, trained quantization and huffman coding. *arXiv preprint arXiv:1510.00149*, 2015. [3](#)
- [9] Ali Hatamizadeh, Yucheng Tang, Vishwesh Nath, Dong Yang, Andriy Myronenko, Bennett Landman, Holger R Roth, and Daguang Xu. Unetr: Transformers for 3d medical image segmentation. In *Proceedings of the IEEE/CVF winter conference on applications of computer vision*, pages 574–584, 2022. [1](#), [6](#), [7](#)
- [10] Geoffrey Hinton, Oriol Vinyals, and Jeff Dean. Distilling the knowledge in a neural network. *arXiv preprint arXiv:1503.02531*, 2015. [2](#), [3](#)
- [11] Andrew G Howard, Menglong Zhu, Bo Chen, Dmitry Kalenichenko, Weijun Wang, Tobias Weyand, Marco Andreetto, and Hartwig Adam. Mobilenets: Efficient convolutional neural networks for mobile vision applications. *arXiv preprint arXiv:1704.04861*, 2017. [3](#)
- [12] Edward J Hu, Yelong Shen, Phillip Wallis, Zeyuan Allen-Zhu, Yuanzhi Li, Shean Wang, Lu Wang, and Weizhu Chen. Lora: Low-rank adaptation of large language models. *arXiv preprint arXiv:2106.09685*, 2021. [2](#)
- [13] Xinrong Hu, Xiaowei Xu, and Yiyu Shi. How to efficiently adapt large segmentation model (sam) to medical images. *arXiv preprint arXiv:2306.13731*, 2023. [3](#)
- [14] Fabian Isensee, Paul F Jaeger, Simon AA Kohl, Jens Petersen, and Klaus H Maier-Hein. nnu-net: a self-configuring method for deep learning-based biomedical image segmentation. *Nature methods*, 18(2):203–211, 2021. [2](#), [5](#), [6](#), [7](#)
- [15] Yuanfeng Ji, Haotian Bai, Chongjian Ge, Jie Yang, Ye Zhu, Ruimao Zhang, Zhen Li, Lingyan Zhanng, Wanling Ma, Xiang Wan, et al. Amos: A large-scale abdominal multi-organ benchmark for versatile medical image segmentation. *Advances in Neural Information Processing Systems*, 35:36722–36732, 2022. [1](#), [6](#)
- [16] Menglin Jia, Luming Tang, Bor-Chun Chen, Claire Cardie, Serge Belongie, Bharath Hariharan, and Ser-Nam Lim. Visual prompt tuning. In *European Conference on Computer Vision*, pages 709–727. Springer, 2022. [2](#)
- [17] Longlong Jing and Yingli Tian. Self-supervised visual feature learning with deep neural networks: A survey. *IEEE transactions on pattern analysis and machine intelligence*, 43(11):4037–4058, 2020. [2](#)
- [18] Alexander Kirillov, Eric Mintun, Nikhila Ravi, Hanzi Mao, Chloe Rolland, Laura Gustafson, Tete Xiao, Spencer Whitehead, Alexander C Berg, Wan-Yen Lo, et al. Segment anything. *arXiv preprint arXiv:2304.02643*, 2023. [1](#), [2](#), [3](#), [7](#)
- [19] Bennett Landman, Zhoubing Xu, J Igelsias, Martin Styner, T Langerak, and Arno Klein. Miccai multi-atlas labeling beyond the cranial vault—workshop and challenge. In *Proc. MICCAI Multi-Atlas Labeling Beyond Cranial Vault—Workshop Challenge*, page 12, 2015. [1](#), [6](#)
- [20] Chengyin Li, Yao Qiang, Rafi Ibn Sultan, Hassan Bagher-Ebadian, Prashant Khanduri, Indrin J. Chetty, and Dongxiao Zhu. Focalunetr: A focal transformer for boundary-aware segmentation of ct images, 2023. [1](#)
- [21] Xin Li, Chengyin Li, and Dongxiao Zhu. Covid-mobilexpert: On-device covid-19 patient triage and follow-up using chest x-rays. In *2020 IEEE international conference on bioinformatics and biomedicine (BIBM)*, pages 1063–1067. IEEE, 2020. [3](#)
- [22] Tsung-Yi Lin, Michael Maire, Serge Belongie, James Hays, Pietro Perona, Deva Ramanan, Piotr Dollár, and C Lawrence Zitnick. Microsoft coco: Common objects in context. In *Computer Vision—ECCV 2014: 13th European Conference, Zurich, Switzerland, September 6–12, 2014, Proceedings, Part V 13*, pages 740–755. Springer, 2014. [1](#)
- [23] Pengfei Liu, Weizhe Yuan, Jinlan Fu, Zhengbao Jiang, Hiroaki Hayashi, and Graham Neubig. Pre-train, prompt, and predict: A systematic survey of prompting methods in natural language processing. *ACM Computing Surveys*, 55(9):1–35, 2023. [2](#)
- [24] Jun Ma and Bo Wang. Segment anything in medical images. *arXiv preprint arXiv:2304.12306*, 2023. [1](#), [3](#), [7](#)
- [25] Maciej A Mazurowski, Haoyu Dong, Hanxue Gu, Jichen Yang, Nicholas Konz, and Yixin Zhang. Segment anything model for medical image analysis: an experimental study. *Medical Image Analysis*, page 102918, 2023. [7](#)

- [26] Sachin Mehta and Mohammad Rastegari. Mobilevit: light-weight, general-purpose, and mobile-friendly vision transformer. *arXiv preprint arXiv:2110.02178*, 2021. **3**
- [27] Bonan Min, Hayley Ross, Elior Sulem, Amir Poursan Ben Veysheh, Thien Huu Nguyen, Oscar Sainz, Eneko Agirre, Ilana Heintz, and Dan Roth. Recent advances in natural language processing via large pre-trained language models: A survey. *ACM Computing Surveys*, 2021. **2**
- [28] Stanislav Nikolov, Sam Blackwell, Alexei Zverovitch, Ruheena Mendes, Michelle Livne, Jeffrey De Fauw, Yojan Patel, Clemens Meyer, Harry Askham, Bernardino Romera-Paredes, et al. Deep learning to achieve clinically applicable segmentation of head and neck anatomy for radiotherapy. *arXiv preprint arXiv:1809.04430*, 2018. **1**
- [29] Maxime Oquab, Timothée Darcet, Théo Moutakanni, Huy Vo, Marc Szafraniec, Vasil Khalidov, Pierre Fernandez, Daniel Haziza, Francisco Massa, Alaaeldin El-Nouby, et al. Dinov2: Learning robust visual features without supervision. *arXiv preprint arXiv:2304.07193*, 2023. **2**
- [30] Junting Pan, Ziyi Lin, Xiatian Zhu, Jing Shao, and Hongsheng Li. St-adapter: Parameter-efficient image-to-video transfer learning. *Advances in Neural Information Processing Systems*, 35:26462–26477, 2022. **2**
- [31] Yao Qiang, Supriya Tumkur Suresh Kumar, Marco Brocanelli, and Dongxiao Zhu. Tiny rnn model with certified robustness for text classification. In *2022 International Joint Conference on Neural Networks (IJCNN)*, pages 1–8. IEEE, 2022. **3**
- [32] Yao Qiang, Chengyin Li, Prashant Khanduri, and Dongxiao Zhu. Interpretability-aware vision transformer. *arXiv preprint arXiv:2309.08035*, 2023. **3**
- [33] Alec Radford, Jong Wook Kim, Chris Hallacy, Aditya Ramesh, Gabriel Goh, Sandhini Agarwal, Girish Sastry, Amanda Askell, Pamela Mishkin, Jack Clark, et al. Learning transferable visual models from natural language supervision. In *International conference on machine learning*, pages 8748–8763. PMLR, 2021. **2**
- [34] Blaine Rister, Darvin Yi, Kaushik Shivakumar, Tomomi Nobashi, and Daniel L Rubin. Ct-org, a new dataset for multiple organ segmentation in computed tomography. *Scientific Data*, 7(1):381, 2020. **6, 1**
- [35] Olaf Ronneberger, Philipp Fischer, and Thomas Brox. U-net: Convolutional networks for biomedical image segmentation. In *Medical Image Computing and Computer-Assisted Intervention—MICCAI 2015: 18th International Conference, Munich, Germany, October 5-9, 2015, Proceedings, Part III 18*, pages 234–241. Springer, 2015. **5**
- [36] Tal Shaharabany, Aviad Dahan, Raja Giryes, and Lior Wolf. Autosam: Adapting sam to medical images by overloading the prompt encoder. *arXiv preprint arXiv:2306.06370*, 2023. **1, 2, 3**
- [37] Mingxing Tan and Quoc Le. Efficientnet: Rethinking model scaling for convolutional neural networks. In *International conference on machine learning*, pages 6105–6114. PMLR, 2019. **3**
- [38] Yucheng Tang, Dong Yang, Wenqi Li, Holger R Roth, Bennett Landman, Daguang Xu, Vishwesh Nath, and Ali Hatamizadeh. Self-supervised pre-training of swin transformers for 3d medical image analysis. In *Proceedings of the IEEE/CVF Conference on Computer Vision and Pattern Recognition*, pages 20730–20740, 2022. **1, 2, 4, 5, 6, 7**
- [39] Wenxuan Wang, Jiachen Shen, Chen Chen, Jianbo Jiao, Yan Zhang, Shanshan Song, and Jianguyun Li. Med-tuning: Exploring parameter-efficient transfer learning for medical volumetric segmentation. *arXiv preprint arXiv:2304.10880*, 2023. **2**
- [40] Xiao Wang and Guo-Jun Qi. Contrastive learning with stronger augmentations. *IEEE transactions on pattern analysis and machine intelligence*, 45(5):5549–5560, 2022. **2**
- [41] Junde Wu, Rao Fu, Huihui Fang, Yuanpei Liu, Zhaowei Wang, Yanwu Xu, Yueming Jin, and Tal Arbel. Medical sam adapter: Adapting segment anything model for medical image segmentation. *arXiv preprint arXiv:2304.12620*, 2023. **1, 3, 7**
- [42] Elad Ben Zaken, Shauli Ravfogel, and Yoav Goldberg. Bitfit: Simple parameter-efficient fine-tuning for transformer-based masked language-models. *arXiv preprint arXiv:2106.10199*, 2021. **2**
- [43] Chaoning Zhang, Dongshen Han, Yu Qiao, Jung Uk Kim, Sung-Ho Bae, Seungkyu Lee, and Choong Seon Hong. Faster segment anything: Towards lightweight sam for mobile applications. *arXiv preprint arXiv:2306.14289*, 2023. **3**
- [44] Chunhui Zhang, Li Liu, Yawen Cui, Guanjie Huang, Weilin Lin, Yiqian Yang, and Yuehong Hu. A comprehensive survey on segment anything model for vision and beyond. *arXiv preprint arXiv:2305.08196*, 2023. **1**
- [45] Kaidong Zhang and Dong Liu. Customized segment anything model for medical image segmentation. *arXiv preprint arXiv:2304.13785*, 2023. **3**
- [46] Yichi Zhang and Rushi Jiao. How segment anything model (sam) boost medical image segmentation? *arXiv preprint arXiv:2305.03678*, 2023. **1**
- [47] Sixiao Zheng, Jiachen Lu, Hengshuang Zhao, Xiatian Zhu, Zekun Luo, Yabiao Wang, Yanwei Fu, Jianfeng Feng, Tao Xiang, Philip HS Torr, et al. Rethinking semantic segmentation from a sequence-to-sequence perspective with transformers. In *Proceedings of the IEEE/CVF conference on computer vision and pattern recognition*, pages 6881–6890, 2021. **5**
- [48] Bolei Zhou, Hang Zhao, Xavier Puig, Sanja Fidler, Adela Barriuso, and Antonio Torralba. Scene parsing through ade20k dataset. In *Proceedings of the IEEE conference on computer vision and pattern recognition*, pages 633–641, 2017. **1**
- [49] Hong-Yu Zhou, Jiansen Guo, Yinghao Zhang, Xiaoguang Han, Lequan Yu, Liansheng Wang, and Yizhou Yu. nn-former: Volumetric medical image segmentation via a 3d transformer. *IEEE Transactions on Image Processing*, 2023. **6, 7**
- [50] Xueyan Zou, Jianwei Yang, Hao Zhang, Feng Li, Linjie Li, Jianfeng Gao, and Yong Jae Lee. Segment everything everywhere all at once. *arXiv preprint arXiv:2304.06718*, 2023. **2**

7. Appendix

We provide supplementary materials in the following relating to the dataset details, processing pipelines, implementation details, and evaluation metrics.

7.1. Dataset Details

A total of 4 CT datasets, including 3 public and 1 institutional dataset, are used to evaluate the performance of models for the 3D multi-organ segmentation task.

BTCV: Beyond the Cranial Vault (BTCV) abdomen challenge dataset [19] includes 30 subjects with abdominal CT scans. In this dataset, 13 organs are annotated by interpreters under the supervision of Vanderbilt University Medical Center radiologists. The multi-organ segmentation task is framed as a 13-class segmentation, which includes large organs such as liver, spleen, kidneys, and stomach; vascular tissues of esophagus, aorta, IVC, splenic, and portal veins; small anatomies of gallbladder, pancreas, and adrenal glands. For the subjects, 24 scans are for training and 6 for testing.

AMOS: We actually use the CT parts in the original AMOS dataset [15], not including their MRI parts. The publicly accessible AMOS-CT dataset [15] consists of 200 multi-contrast abdominal CT scans for training and 100 for testing. These scans are annotated for 15 anatomies, including spleen, right kidney, left kidney, gallbladder, esophagus, liver, stomach, aorta, inferior vena cava, pancreas, right adrenal gland, left adrenal gland, duodenum, bladder, and prostate/uterus.

CT-ORG: CT Organ Segmentation Dataset (CT-ORG) [34] comprises 100 CT scans, each of which includes ground-truth contours of 5 different organs (lungs, liver, bladder, kidney, and pelvic bones). Of these, the first 19 CT datasets are exclusively reserved for testing purposes whereas the remaining 81 are used for model training [34].

Institutional Pelvic: In addition to public datasets, we also test the performance of the segmentation models on a private dataset. An institutional pelvic dataset of 300 prostate cancer patients is retrospectively selected, and each contains 3 manually generated contours (prostate, bladder, and rectum). The 300 cases are randomly split into a training set of 225 cases, a validation set of 30, and a testing set of 45. Institutional review board (IRB) approval was obtained for this study.

7.2. Preprocessing Pipelines

For each dataset, we perform interpolation for a fixed voxel spacing over all scans within this dataset, then intensity normalization, sampling over positive and negative patches, and finally data augmentation. We provide additional parameters for each dataset as follows:

BTCV: All CT scans are interpolated into the voxel spacing of $[1.0 \times 1.0 \times 1.5]$ mm. A Hounsfield unit (HU)

range of $[-125, 275]$ is clipped from the raw inputs and then normalized to the interval $[0, 1]$ followed by random sampling of $128 \times 128 \times 128$ voxels. Data augmentation of random flip, rotation, and intensities scaling are used for training, with probabilities of 0.1, 0.1, and 0.2, respectively.

AMOS: Each CT scan is interpolated to a voxel spacing of $[1.0 \times 1.0 \times 1.5]$ mm, HU values for each scan in the AMOS dataset are clipped to the range $[-991, 362]$. Subsequently, truncated voxel values are normalized by subtracting 50 and dividing by 141. 3D patches of $128 \times 128 \times 128$ voxels are obtained by sampling positive and negative ratio of 1 : 1. A probability of 0.1 is used for random flip and rotation, and 0.2 for intensities scaling.

CT-ORG: Each CT dataset was interpolated to the isotropic voxel spacing of 2.0 mm. Intensities are scaled to a HU range of $[-1000, 1000]$, then normalized to $[-1, 1]$. We sample the training sub-volumes of $128 \times 128 \times 128$ voxels by a ratio of positive and negative as 1 : 1. Augmentation probabilities for random flip rotation, intensities scaling, and shifting are set to 0.5, 0.5, 0.1, and 0.1, respectively.

Institutional Pelvic: We interpolate each image to isotropic voxel spacing of 1.5 mm. and a Hounsfield unit (HU) range of $[-50, 150]$ is used and normalized to $[0, 1]$. Subsequently, training samples are cropped to a $128 \times 128 \times 128$ voxel patch around the prostate/bladder/rectum regions. Augmentation probabilities of 0.3, 0.2, 0.1, and 0.1 are used for random flip rotation, intensities scaling, and shifting.

7.3. Implementation Details

All experiments and comparisons employ **SAM-B**, utilizing **ViT-B** as the backbone for the image encoder. Model training is conducted with a batch size of 1 on NVIDIA A100 GPUs. For the 200 epochs training with AdamW optimizer, we incorporate the first 5 epochs for warmup.

7.4. Evaluation Metrics

We utilize the Dice similarity coefficient (Dice) and Normalized Surface Distance (NSD) [28] as metrics to evaluate the segmentation performance. Dice metric measures the extent of agreement between two volumes with the following formula:

$$\text{Dice} = \frac{2 \sum_{i=1}^I g_i \hat{g}_i}{\sum_{i=1}^I g_i + \sum_{i=1}^I \hat{g}_i}, \quad (1)$$

where g and \hat{g} denote the ground truth and the predicted voxel values. The NSD metric quantifies the overlap between ground truth and predicted surfaces (with a fixed tolerance). For both metrics, 0 denotes the worst match between two structures, and 100% means the perfect match.